Received March 2, 2022, accepted April 18, 2022, date of publication April 22, 2022, date of current version May 2, 2022.

Digital Object Identifier 10.1109/ACCESS.2022.3169489

Determination of Control Requirements to Impose on CIG for Ensuring Frequency Stability of Low Inertia Power Systems

BENJAMÍN VEGA[1], CLAUDIA RAHMANN[1], (Member, IEEE), RICARDO ÁLVAREZ[2], (Member, IEEE), AND VIJAY VITTAL[3], (Life Fellow, IEEE)

[1]Department of Electrical Engineering, University of Chile, Santiago 8320000, Chile
[2]Department of Electrical Engineering, Universidad Técnica Federico Santa María, Santiago 8940000, Chile
[3]Department of Electrical, Computer and Energy Engineering, Arizona State University, Tempe, AZ 85281, USA

Corresponding author: Claudia Rahmann (crahmann@ing.uchile.cl)

This work was supported in part by the Chilean National Agency for Research and Development [Agencia Nacional de Investigación y Desarrollo (ANID)] under Grant ANID/FONDECYT/1201676, Grant ANID/Fondap/15110019, and Grant ANID-Subdirección de Capital Humano/Magíster Nacional/2019 - 22191313.

ABSTRACT Power systems around the globe are undergoing a transformation characterized by a massive deployment of converter-interfaced generation (CIG) to effectively combat climate change. However, achieving a seamless transition from current power systems dominated by synchronous generators (SGs) to future ones with high levels of CIG requires overcoming several technical challenges. From a frequency stability perspective, reduced system inertia increases the frequency nadir after a loss of generation thereby endangering frequency stability. In this context, this paper proposes a novel methodology for determining control requirements to impose on CIG as their penetration in the network increases. Results of a case study based on the Chilean grid projected for the year 2046 show that, if only grid-following converters without frequency control capability are deployed, a maximum CIG penetration level of 75% can be achieved without threatening frequency stability. The Chilean system can reach a 99% CIG penetration, provided that the remaining CIGs are deployed in grid-following with frequency support capability. Finally, we show that if the last SG is replaced with a grid-forming converter, the system can still sustain frequency stability and exhibits a good dynamic performance. These results demonstrate that, at least from a frequency stability viewpoint, achieving a 100% based CIG system is technically possible. The proposed methodology can be used by energy regulators to define the control requirements necessary to impose on CIG for achieving renewable energy targets in a secure way. Although the obtained results are particular for the Chilean system, the proposed methodology can be applied to any power system.

INDEX TERMS CIG, grid-following converter, grid-forming converter, frequency stability, low-inertia systems, PLL, renewable energy resources.

NOMENCLATURE

A. SYMBOLS

Δ_{CIG}	Block of CIG displaced by SG (MW).
i_{max}	Maximum number of iterations for an iterative process.
Max_{CIG_gf}	Maximum penetration of grid-following CIGs (%).
$Max_{CIG_{gf}+f}$	Maximum penetration of grid-following CIGs with a frequency controller (%).
CIG_{target}	Penetration target of CIG (%).
y_{target}	Year with a defined CIG penetration target.

B. PARAMETERS

m	Droop coefficient for the frequency controller of a CIG (%).
n	Droop coefficient for the voltage controller of a CIG (%).
K_{vi}	Integral gain of the voltage controller of a grid-following CIG (pu).
K_{iPLL}	Integral gain of the PLL of grid-following CIGs (pu).

The associate editor coordinating the review of this manuscript and approving it for publication was Inam Nutkani.

K_{vp}	Proportional gain of the PI voltage controller of grid-following CIGs (pu).
K_{pPLL}	Proportional gain of the PLL of grid-following CIGs (pu).

C. PERFORMANCE INDICATORS

ξ	Damping ratio of an eigenvalue (%).
f_{nadir}	Frequency nadir following a contingency (Hz).
ξ_{min}	Minimum damping ratio of the eigenvalues obtained (%).
T_s T_{nadir}	Settling time of the frequency following a contingency (s) Time for reaching the frequency nadir after a contingency (s).

I. INTRODUCTION

A. AN ENERGY TRANSITION IS ALREADY UNDERWAY

The diverse effects that climate change has had on the environment have motivated several countries to promote strong power policies with the aim of decarbonizing their electrical energy systems. Among the pillars for achieving this ambitious objective are an accelerated deployment of renewable energy sources (RES), as well as different energy efficiency measures [1], [2]. The results of said policies are already evident: since 2010, the cumulative renewable energy capacity (including hydropower) rose worldwide from 1227 GW to 2799 GW by the end of 2020 [3], [4]. This growth has been especially high for RES based on power converters, such as solar photovoltaic (PV) and wind power (WP) generation. Between 2009 and 2019, the installed capacity of both technologies has grown in factors of 40 and 6 respectively [5], [6], and the projections indicate that this upward trend will further continue in the coming years [7], [8]. In what follows, when referring to any kind of converter-based RES such as PV and WP, the term CIG will be used, following the terminology used in the recently published report of the IEEE Power System Dynamic Performance Committee [9].

While the transition to low-carbon electricity systems is already underway, achieving it seamlessly is not an easy task. Several studies and practical experiences worldwide have shown that to make this transition safely, the energy sector must first jointly overcome enormous technical challenges not only related to the stochastic nature of RES [10], but also to technical features of the power electronic converters of these energy resources [11], [12]. Although both aspects have wide-ranging repercussions in power systems operation and control, major challenges stem from the underlying dynamic behavior of CIG and its substantial differences with conventional generation facilities. Among the cornerstones to understand this are:

- *Fast response of converters*: The dynamics of power converters and their controls are significantly faster than the ''slow'' electromechanical dynamics of SGs and their control systems [9], [13]. Consequently, the dynamic response of power systems dominated by CIG becomes faster and hence more difficult to control [13]. From a frequency stability perspective, this may lead to situations in which traditional protection schemes become too slow to prevent large frequency deviations [14]. Furthermore, fast phenomena within the electromagnetic time scale (usually neglected in stability analysis), may become relevant [9], meaning that fast control interactions due to dynamic couplings between the converters and the grid are more likely to arise [2].
- *Dependency on control strategy*: The overall dynamic performance of CIGs, along with their interaction with the grid during contingencies, is dominated by the control systems and strategies used to control the power electronic converter interface between the energy source and electric grid [1], [2], [9], [11]. This contrasts with conventional synchronous generators (SGs), where the physical properties of the machine itself, such as inertia and electrical parameters, play the largest role in determining their transient behavior [1]. This high dependence on the control strategy means that the dynamic performance of CIG during contingencies will substantially vary not only depending on system operating conditions and fault characteristics, but also on the chosen control strategy, parameters, and equipment vendor.

Aside from the two factors mentioned above, as the penetration of converter-based RES grows, hundreds (or even thousands) of new fast-control points are created in the grid [15], which inevitably adds a supplementary layer of complexity in terms of coordination, monitoring and (cross) parameter tuning.

B. CHALLENGES FROM A FREQUENCY STABILITY PERSPECTIVE

The stability problems of power systems with high levels of CIG cover a wide spectrum of phenomena, which may range from timescales of a few seconds to minutes, or even hours [9], [13]. In this section, we summarize the stability challenges with a focus on frequency stability and related control issues. Other relevant challenges such as voltage stability, converter-driven stability (including slow- and fast-interactions), and electric resonance stability [9], [16] are out of the scope of this article and hence are not further discussed.

From a frequency stability perspective, several studies have shown that system dynamic performance can be seriously threatened by CIG power plants due to their lack of inertial response [14], [17] and by the significantly faster response of converters in comparison to conventional SGs [11], [13], [18]. Reduced system inertia increases the frequency deviation after a loss of generation and leads to a steeper rate of change of frequency (RoCoF) at the inception of a contingency [17], [19], [20], which means that the system frequency dynamics become faster [2], [14]. This can make conventional frequency control schemes too slow to successfully

overcome large frequency deviations, which could cause a more frequent activation of the under-frequency load shedding schemes (UFLSS), thereby risking the security of the electricity supply [12].

Although the lack of inertial response can be counteracted through fast-acting energy storage systems [1], [21] or additional control loops in the CIG converters [17], [22], the underlying mechanism behind such support also raises challenges. This is because the frequency support provided by CIGs is a fully actuated response implemented through a control loop, and hence it is subject to actuation delays, poor tuning of parameters, possible malfunctions, current saturation of the converters, as well as potential (unstable) fast control interactions that are difficult to predict [2]. Conversely, the support of SGs during the first seconds after a power imbalance (inertial response) is based on the available kinetic energy naturally stored in their rotating masses according to Newton's second law of motion [11], [12], [23]. This support is, therefore, naturally coupled to the physical principles governing the machine's behavior, and hence, intrinsically ensured.

From a frequency stability perspective, the secure transition from up-to-date bulk power systems to low-inertia grids dominated by CIG is essentially a complex control problem. Accordingly, a first step is to conceive how to successfully coordinate thousands of fast-response CIGs distributed throughout the grid while, at the same time, operating them successfully in parallel with few (dispersed) synchronous machines.

C. OPEN RESEARCH QUESTION

Power electronic converters are modular and nearly fully actuated devices that allow a wide variety of control alternatives with very fast actuation times [2], [9]. Grid-following and grid-forming are the most frequently mentioned operating modes in the literature. Still, grid-forming converters have essentially been used in microgrid applications only, without being deployed in bulk power systems [24]. Other operating modes such as partial grid-forming [25], grid supporting [26], [27] or combinations thereof are also conceivable, thus further increasing the control alternatives of these devices.

Currently, the dominant operating mode used by vendors in CIG-based power plants is the grid-following mode [1], [2], [7]. In their most basic form, grid-following converters inject a fixed amount of power just *following* the imposed voltage and frequency of the grid, meaning that the output power does not change as a function of the system operating condition. Accordingly, it is highly unlikely that future power systems with low inertia levels could ever operate just with grid-following CIG in its most basic form. Although modern grid-following converters can be easily programmed to embed frequency and voltage control capabilities [28]–[30], as their penetration in the network increases, some CIG units will have to be operated as grid-forming in order to participate in the process of forming frequency and voltage [2], [31]. Moreover, grid-following converters have limited restoration-support capabilities because they depend on an external source for regulating system frequency and voltages [24]. Still, as long as no cost-effective grid-forming solution for high-voltage applications is developed, grid-following CIG with frequency/voltage controllers will continue to be the best option for enabling the widespread integration of CIG without threatening system stability.

The *control flexibility* of power electronic converters offers a wide range of opportunities, but it also raises many questions and new paradigms that are yet to be addressed. For instance, open questions are: what are the control requirements that need to be imposed on CIG-based power plants as their penetration in the network increases? When should grid-following CIG compulsorily embed frequency and voltage control capabilities? From which point onward should it be mandatory for new CIGs to be operated as grid-forming resources? So far, the most realistic scenario that can be conceived to successfully operate low-inertia power systems, is one in which a mix of grid-following, grid-following with frequency/voltage control capability, and grid-forming converters coexist. However, it is unclear at which penetration level of CIG should *more advanced* operating modes be required to ensure stability, or the ways in which these requirements change depending on power system characteristics and CIG deployment.

D. WHAT HAS BEEN DONE

To date, several studies and magazine articles have been published addressing different control challenges that power systems with high levels of CIG will face. Although useful insights and results have been obtained so far, no work has directly addressed the question of how energy regulators should define the control requirements that CIG must fulfill as their penetration in the network increases. Next, we discuss main results and conclusions of recent studies that are closely related to our work. Even though these studies do not have our same objective, they still provide useful results and conclusions for our work.

One significant drawback of recent works that address control challenges in low-inertia power systems is that most of them use small test systems modeled with a few equivalent generators and busbars [7], [32]–[34]. In these cases, drawing general conclusions applicable to real-world power systems is difficult. Among the research applicable to large-scale real power systems, [32] and [35] compare the dynamic performance of 100% renewable power systems using different types of grid-forming controllers. In particular, the work in [32] includes droop control, virtual synchronous machines, matching control, and virtual oscillators. The results of [32] show that regardless of the chosen grid-forming control strategy, the frequency performance is improved when using grid-forming CIGs compared to SGs. Moreover, both works conclude that multiple grid-forming control schemes can coexist in the same power system, provided that all of them show similar behavior and are compatible with each other. In the context of the MIGRATE project [36], [7] presents

an analysis of the operational limits and the minimum grid-forming converters penetration required to maintain voltage stability during short-circuits. For this, a reduced model of the Irish system operated with a 100% CIG penetration is used. To find the minimum grid-forming penetration level, first a 100% grid-forming CIG system is implemented. Then, grid-forming CIGs are progressively displaced by grid-following ones until the system becomes unstable. The results show that for the Irish system, a minimum grid-forming CIG penetration of 37.5% is needed to sustain voltage stability. This limit can be reduced to 30.1% if the grid-forming capacity is distributed more evenly across the grid. A similar study is presented in [37] for the Western Electricity Coordinating Council (WECC) 2012 system (consisting of 18205 buses). This work focuses on transient stability for a grid with a CIG penetration close to 100%. The converters are modeled as grid-following sources with frequency droop controllers. This work shows that a power system with very low inertia can remain stable for different types of contingencies when grid-following converters are used.

The works [7], [32], [35], and [37] presented before show that it is possible to sustain voltage and rotor-angle transient stability in power systems with very high levels of CIG. Regarding studies with focus on frequency stability, not much has been done. In [12], the feasibility of operating a 100% CIG-based system during power imbalances is studied. The results show that grid-following converters with traditional frequency droop control do not contribute to the load sharing process when a grid-forming CIG imposes a constant frequency. In this respect, the authors conclude that if angle droop controllers [38] are used instead, the system can operate with a constant frequency while ensuring proper load sharing among units. Hence, an important conclusion of this work is that a 100% CIG-based system can indeed be operated at a constant frequency without the need of secondary frequency controllers.

E. CONTRIBUTIONS OF THIS WORK

As presented in the previous section, to the best of the authors' knowledge, no work has proposed a methodological approach to systematically define the control requirements that grid-connected CIG must fulfill to enable its widespread adoption from a frequency stability viewpoint. In this context, this work proposes a novel methodology to systematically define the control requirements that must be imposed on CIG-based power plants as their penetration in the network increases. The methodology is designed to ensure frequency stability during extreme contingencies assuming that: 1) in a first stage of CIG development (in which no major frequency challenges arise), CIGs are operated in grid-following mode without any frequency control, 2) in an intermediate stage of deployment, at least some CIG units will be required to participate in system frequency regulation and then, 3) as the system inertia approaches zero, some CIG will also be required to participate in the process of forming frequency and voltage. The study is based on time-domain simulations using a complete dynamic model of the Chilean system projected to the year 2046. The Chilean case is particularly interesting because it already has high levels of solar power concentrated in the north of the country and it is an isolated extreme longitudinal network prone to face stability problems. Although our results and conclusions are only valid for the Chilean case, the proposed methodology can be applied to any other power system. Our study provides several useful insights to start outlining answers to the following questions:

- What is the maximum level of grid-following CIG that a system can accommodate without compromising frequency stability?
- When should CIG be required to embed frequency control capabilities?
- If the system includes grid-following CIG with and without frequency control capability, from which point onward should it be required that new CIG be operated as grid-forming devices?

The remainder of the paper is organized as follows. In Section II the main characteristics of the most common converter operating modes are summarized. The methodology used for the study is presented in Section III. In Section IV the case study implemented is described. Finally, results are discussed in Section V and the conclusions are presented in section VI.

II. OPERATING MODES OF CONVERTERS

As mentioned in the introduction, power converters used in CIG power plants allow a variety of operating modes. Although the names that are most repeated in literature are grid-forming and grid-following modes, different names can also be found (e.g., the grid-following mode has also been called grid-feeding [26], [39]). Next, we present the main characteristics of the most common operating modes of power electronic converters.

A. GRID-FOLLOWING CONVERTERS

The vast majority of converters used in existing CIG power plants rely on an external voltage source to operate and also on a phase-locked loop (PLL) to estimate the angle of the measured voltage at the connection point of the converter. They require a stiff grid (robust grid), whose voltage and frequency at the connection point can be determined by a PLL. This family of converters is often referred to as grid-following converters [1], [2]. In the traditional grid-following operating mode, the converter is controlled as a current source that injects a fixed amount of active and reactive power to the grid by simply *following* the voltage and frequency at its connection point [7], [12], [26]. Consequently, the use of grid-following converters is feasible as long as the system to which the CIG is connected has other generators capable of participating in the process of establishing the frequency and voltage of the network [1], [7], [24].

The control scheme of a grid-following converter can be implemented in different ways [26]. In the area of power

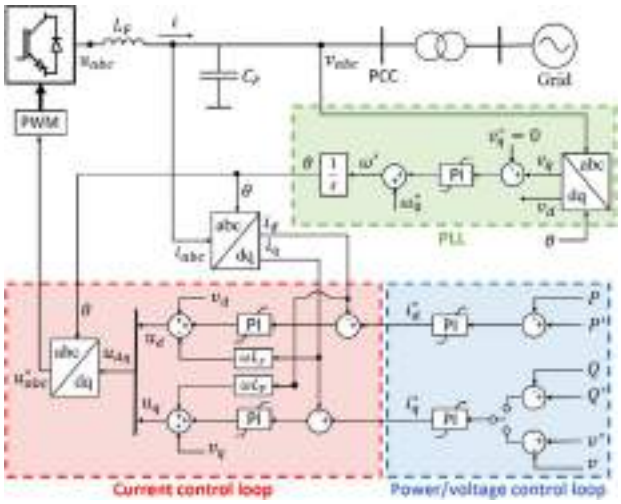

FIGURE 1. Generic control structure of a grid-following converter.

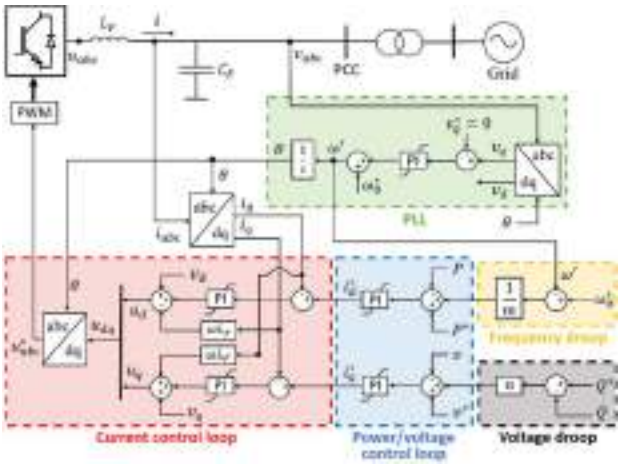

FIGURE 2. Generic control structure of a grid-following converter with droop controllers.

systems, PI (Proportional-Integral) controllers are used the most, as well as systems in *dq* axes [40]–[42]. Fig. 1 illustrates a typical control diagram of a grid following converter. This scheme has two cascaded control loops based on PI controllers oriented in the *dq* axis. The angular reference of these axes comes from a PLL. Although the synchronous reference frame PLL (SRF-PLL) is currently the most widely used method by vendors to synchronize CIGs to the grid [43]–[45], other synchronization alternatives such as adaptive-based PLLs [46], the decoupled double SRF-PLL (DDSRF-PLL) [47], the dual SRF filtering-based PLL (DSRF-PLL) [48], or the dual complex-coefficient filter-based PLL (DCCF-PLL) [45], have also been proposed. Further, PLL adaptations without direct computation of trigonometric functions [49] and implementations using the Kalman filter [50] or the recursive Discrete Fourier Transform (RDFT) [51] are also among the newer synchronization solutions proposed in the literature.

In this case, the PLL estimates the phase (θ) of the voltage at the point of common coupling (PCC). This angle is used to transform current and voltage measurements from the *abc* axes to the *dq* axes. The orientation of the *dq* axes is regulated using a PI loop that carries the voltage of the *q*-axis (v_q) to zero. This ensures that the voltage at the PCC is aligned with the voltage in the *d*-axis (v_d) [43], [52].

The external control loop regulates the active power injected (P) by manipulating the current in the d-axis (i_d), while simultaneously regulating either the reactive power injected (Q) or the magnitude of the voltage at the PCC (v) through the current in the qq-axis (i_q). For this, PI loops are used, which, from the errors between reference values and measured power/voltage, determine the reference currents to be injected in *dq* axes $\left(i_d^*, i_q^*\right)$. These reference currents are used by the internal control loop to regulate the current injected by the converter. The output of the current internal loop is the voltage u_{abc}^* that has to be imposed at the converter terminals in order to inject the desired values of active and reactive power.

Although the basic control structure explained above was the most common until recently, as discussed in [25], additional modes of operation are also feasible. For example, in [11], [53], [54], grid-following converters with control loops designed to regulate voltage magnitude instead of the reactive power injected are considered. This form of operation is known by some authors as partial grid-forming [25]. Other research works have proposed to incorporate external loops into the classic grid-following control schemes for CIG to participate in frequency and/or voltage regulation [27], [33]. Grid-following converters with frequency/voltage controllers have not only been discussed by the academic community, but have already been required and implemented in several power systems [28]–[30].

A possible control scheme for a grid-following converter with frequency and voltage droop control is presented in Fig. 2 [27]. Although in some research articles this implementation is known as grid-supporting operating mode [26], [27], in this work we refer to this implementation as grid-following converter with droop controllers. As shown in Fig. 2, when the frequency measured by the PLL (ω') differs from the nominal frequency (ω_0^*) (e.g., due to a load imbalance in the grid), the frequency droop modifies the value of the active power P^{**} to be injected. This way, the converter contributes to restoring the balance between generation and demand, similar to the action of governors in conventional SGs [33]. Similarly, the voltage droop determines a new reference voltage v^{**} based on the reactive power deviation measured at the PCC so that the CIG participates in the voltage regulation.

The control action of the frequency and voltage droop controllers are represented in (1) and (2), respectively, where the droop gains m and n determine the converter contribution to the frequency and voltage regulation.

$$P^{**} = P^* + 1/m \cdot (\omega_0^* - \omega') \tag{1}$$

$$v^{**} = v^{*} + n \cdot (Q^{*} - Q) \tag{2}$$

To ensure frequency support during power imbalances (1), the converters must keep some power reserves available. This can be done either by incorporating an energy storage system [55] or by operating the converters in de-load mode [1], [10], [22]. When operating in de-load mode, the CIGs only supply a percentage of the available power, meaning that they operate at a sub-optimal operating point and not at the maximum power point commonly used in traditional grid-following CIGs with no frequency response capability [10].

Although the incorporation of these additional control functionalities allows grid-following converters to contribute to system recovery following a loss of generation, their support capability is quite limited, as they still depend on a stiff (well-defined) terminal voltage that the PLL can follow. Regardless of the grid-following control structure used, black-start following a system outage could represent a significant challenge in low-inertia power systems where most SGs have been replaced with grid-following CIGs [24].

B. GRID-FORMING CONVERTERS

The term "grid-forming" is generally used to refer to generation plants that are able to impose frequency and voltage autonomously without the need of an external grid [11], [26]. Conventional synchronous machines are the grid-forming generation sources *par excellence*. In the case of CIG, power plants with similar functionalities to SGs are generically referred to as grid-forming CIGs. Similarly, to SGs, grid-forming converters have black-start capability and can contribute to system restoration following a blackout [24]. Accordingly, the grid-forming operating mode can, at least theoretically so far, operate in a power system without any conventional SG [26], [31], [35]. Nevertheless, today there is not enough experience with grid-forming converters operating in real power systems.

Grid-forming converters can be implemented in several ways [32]. Although the most well-established grid-forming method is the droop control [7], there are also other strategies such as virtual synchronous generators (also called synchroinverters) [56], [57], virtual oscillator [58], [59], and matching control [35], [60], to name a few. However, these methods are not discussed further here as they are not the focus of this work, and they have been proven to be mathematically equivalent to the classic droop control [35], [39], [61].

Fig. 3 shows a generic control scheme for a grid-forming converter with droop-type controllers. The diagram has three cascaded control loops oriented in the dq axis. In contrast to a grid-following converter, this operating mode does not need a PLL for synchronizing the converter to the grid [39], [62], [63]. Instead, the angle θ, which defines the dq axis orientation, is obtained by integrating the reference frequency that the converter imposes at the PCC [62].

The droop controller is the outer loop of the scheme in Fig. 3. This controller allows the converter to participate

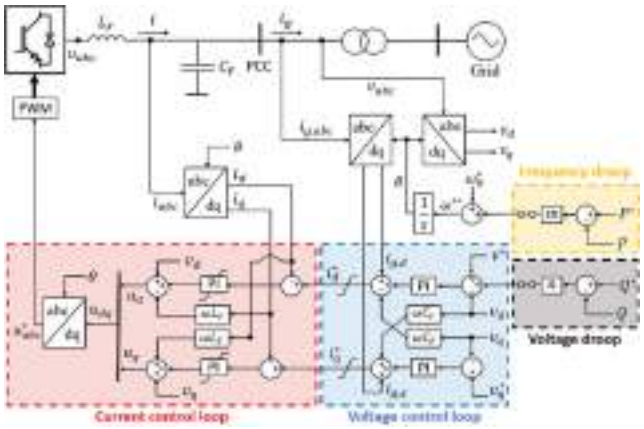

FIGURE 3. Generic control structure of a grid-forming converter.

in the frequency and voltage regulation, and therefore, in load distribution among generators [53], [64]. The frequency loop of a grid-forming converter is represented in (3).

$$\omega^{**} = \omega_0^{*} + m \cdot (P^{*} - P) \tag{3}$$

where ω^{**} is the reference frequency to be imposed at the PCC, ω_0^{*} is the reference frequency when the converter injects the reference power P^{*}, and P is the active power injected in the grid. When a disturbance leads to a deviation in the active power injected by the converter ($P^{*} \neq P$), the droop control modifies the output frequency imposed by the converter according to the deviation of power injected and the droop coefficient m [62]. Once the steady state is reached, the generators distribute the load variations according to the slope of their droop curves [26]. This controller is also known as "inverse droop", because, as opposed to the governor of an SG, it modifies the output frequency considering the deviation of the injected power in relation to its reference [65]. As in the case of grid-following converters, the frequency regulation capability in grid-forming mode requires an energy buffer (power reserve), which can be achieved by either incorporating an energy storage system or by operating the converters in de-load mode.

Similarly, the voltage magnitude established at the PCC is modified according to (4).

$$v^{**} = v^{*} + n \cdot (Q^{*} - Q) \tag{4}$$

The frequency and voltage references provided by the droop controllers enter to the voltage control loop where, from the voltage measurement at the PCC and from the current i_g injected into the grid, the reference currents $\left(i_d^{*}, i_q^{*}\right)$ to be injected to the grid by the converter are calculated. These reference values are the input of the internal current control loop, which determines the voltage u_{abc}^{*} to be imposed at the converter terminals to establish the desired voltage at the PCC.

III. PROPOSED METHODOLOGY

A. INTRODUCTION

As mentioned in the introduction, this paper proposes a novel methodology to systematically define the control requirements imposed on CIGs to ensure system frequency stability as their penetration in the network increases. To this end, it is assumed that the corresponding power system under study has a CIG penetration target (CIG_{target}) for a year y_{target} in the future, for which there is an elaborated roadmap for the expansion of its generation matrix. On this basis, the proposed methodology consists of three main stages that are briefly explained next.

1) *Maximum level of CIG in grid-following mode only (business-as-usual):* in this stage, the purpose is to determine the maximum level of CIG penetration, assuming that these units are connected in a grid-following mode only, i.e., without any frequency control. The assumption behind this is that in the first stage of CIG deployment, in which there are no major effects on the frequency stability of the system, the CIGs will be connected to the network in grid-following mode, as this is the default control scheme used today in nearly all grid-connected CIGs due to its maturity, economic advantages and collected practical experience.
2) *Maximum level of CIG in grid-following+f mode:* in this stage the system obtained in stage one is taken as a base, and the penetration of CIG is increased provided that new units participate in system frequency regulation. Here it is assumed that once the energy regulators start demanding capacity of frequency regulation in the new CIGs, the solution that vendors will adopt will simply be to add a frequency loop to the traditional grid-following mode.
3) *Maximum level of CIG considering grid-forming mode:* in this last stage, the system obtained in stage 2 is taken as a base, and the CIG level is increased provided that the new CIG power plants being incorporated into the system are connected in grid-forming mode. Accordingly, these CIGs must support the process of forming frequency and voltage and also contribute with black-start capability.

As will be explained in detail in the next sections, in each of these three stages, the determination of the maximum level of CIG is done through an iterative process in which the dynamic performance of the system is continually assessed for different levels of CIG. The performance assessment includes a small-signal stability assessment (modal analysis) and a dynamic assessment through time-domain simulations during large disturbances. The method described is illustrated in Fig. 4. Note that the proposed methodology is general enough to be applied to any power system. The main requirement is to have available both an appropriate dynamic model of the network for time-domain simulations and a penetration target of CIG.

The process mainly consists of increasing the CIG level and, for each penetration level, assessing if the power system has a good dynamic performance. If the performance is satisfactory, the CIG penetration is increased in Δ_{CIG} and the system performance is assessed again. This iterative process is repeated until for a certain CIG level the system becomes unstable, or the maximum number of iterations i_{max} to make the system stable (for a certain CIG level) is exceeded.

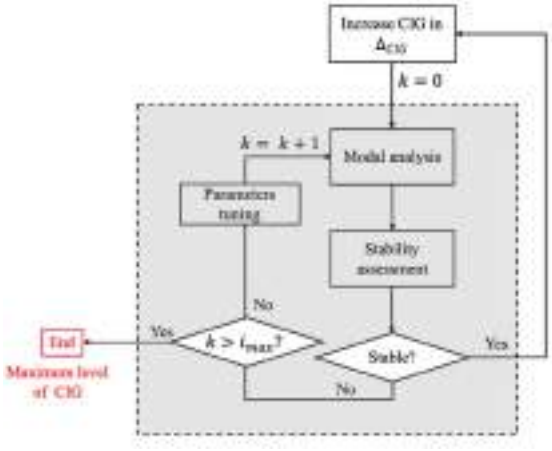

FIGURE 4. General block diagram.

In the following subsections, each methodological stage is presented in detail. In addition, an initial section called ''First steps'' is included to present some general considerations about the dynamic studies.

It is worth to mention that each time that the term ''grid-following'' is used, we are referring to converters operating in a grid-following mode in its most basic form, that is, without any kind of frequency control. To refer to the case of grid-following converters with some frequency controller, we will use the term ''grid-following+f''.

B. FIRST STEPS

In what follows, some practical aspects of the dynamic study that is undertaken in each of the three stages of the proposed methodology are addressed.

1) BASE DYNAMIC MODEL OF THE SYSTEM

As a first step before beginning with Stage 1 of the methodology, the dynamic model of the projected system to the year y_{target} for which there is a defined CIG target (CIG_{target}) must be elaborated. For the current roadmap with the generation expansion plan of the system (that allows to reach said objectives) is used alongside any other official information from regulator and/or transmission system operator (TSO). Based on this first system model, all future CIG power plants are (initially) modeled in grid-following mode. This initial model is called $Model_{v0}$.

2) FREQUENCY CONTROL AREAS

For the purposes of the dynamic study, the power system is divided in frequency control areas, which may be determined either using any existing methodology [33], [66], [67]

or based on the practical experience of the pertinent TSO. Regardless of the method used, this step is a *must*, so that potential problems with inertia distribution can be addressed [14], [66], [68]. As explained in [14], [66], [68], in low inertia power systems, post-fault frequency dynamics do not only depend on the total system inertia, but also on their spatial distribution across the network. As a consequence, not including this division in the system may compromise the validity of the obtained results.

3) SYSTEM OPERATING CONDITIONS AND CONTINGENCIES

As is common in stability assessments of large-scale power systems, we adopt a *worst-case approach*, meaning that only a limited set of critical operating points and contingencies are investigated [69]. Since frequency stability problems are more likely to arise during periods of low system inertia [2], [17], the study is undertaken for the minimum net load operating point (i.e., when SGs generate the least amount of power), in which case only few SGs are available to support the system frequency response. Regarding the contingencies to be studied, the sudden outage of the largest online generation unit [70] is considered, since this contingency is critical from a frequency stability perspective. In addition, to evaluate the technical feasibility of reaching high levels of CIG penetration, the set of critical contingencies to be analyzed include the sudden disconnection of the wind and PV power plants with the greatest generated power in the corresponding operating condition.

4) PERFORMANCE INDICES

In regard to the dynamic performance indicators that are used in this study, we have that:

- For the small-signal stability assessment, it is demanded that all eigenvalues obtained must be stable and with a damping ratio complying with $\xi_{min} > 10\%$. In this paper, that value is used because it is the minimum established in the Chilean grid code [71]. However, depending on the case under study, and the corresponding regulations, this value may change.
- To assess the dynamic performance of the system during large power imbalances, two indicators are used: (i) the minimum frequency (nadir) reached following each fault and (ii) the settling time of the frequency in its post-fault steady state value. The boundary values for both indicators are obtained from current regulations.

C. STAGE 1: MAXIMUM LEVEL OF CIG IN GRID-FOLLOWING MODE ONLY (BUSINESS-AS-USUAL)

The objective of the first stage in this methodology is to determine the maximum level of CIG operating in grid-following mode (Max_{CIG_gf}) that can be incorporated into the system while maintaining stability. For this, the model $Model_{v0}$ is taken as a base. Then, an iterative process is performed, which consists of 2 cascaded stages whose details are presented in what follows.

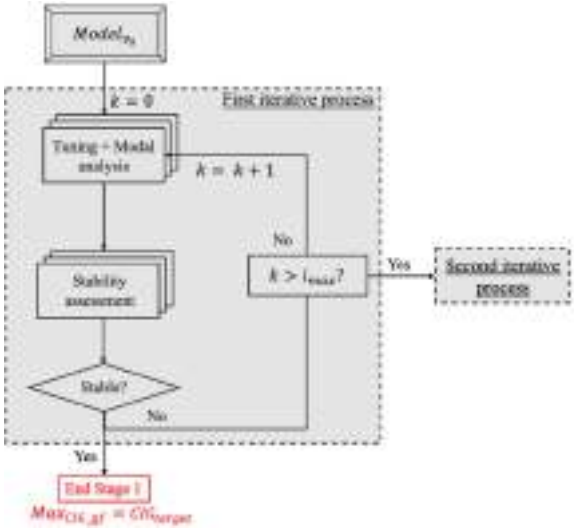

FIGURE 5. Block diagram of first iterative process of Stage 1.

1) FIRST ITERATIVE PROCCESS

Through this first process, we seek to verify if the target defined (CIG_{target}) for the year y_{target} can be reached only based on grid-following converters. For this, the iterative process shown in Fig. 5 is followed, where each iteration includes a tuning process based on a modal analysis, followed by a stability assessment.

The tuning process performed in each iteration k considers the parameters of the CIG controllers, including the bandwidth of the PLLs and the gains (K_{vp}, K_{vi}) of the PI controllers in the voltage control loop. Additionally, the process may include the retuning of some Power Systems Stabilizers (PSS) of conventional machines through the modification of their gains, K_{PSS}. The parameter tuning is made based on several modal analyses using a trial-and-error process. The tuning in iteration k ends when the system reaches a suitable performance in small signal, that is, when all system eigenvalues are stable with damping ratios complying with $\xi_{min} > 10\%$. Once the system has been tuned, the stability analysis begins. This analysis is made through time-domain simulations where the critical contingencies of each frequency control area are simulated. If for one of the contingencies the system becomes unstable and/or its dynamic performance does not comply with the corresponding technical regulation, the following iteration is conducted and the process that was previously described starts once again, that is, the parameters are retuned, and again, a stability analysis is conducted.

This first iterative process ends when one of the following conditions is met:

- If for an iteration $k \leq i_{max}$ the system dynamic performance complies with current regulation, and it is stable during all critical contingencies, the iterative process ends, and it is therefore concluded that the CIG_{target} can be reached only using CIG in grid-following mode alone. Accordingly, the maximum

level of penetration of these units is equal to the target, i.e., $Max_{CIG_gf} = CIG_{target}Max_{\text{CIG_gf}}$ = CIG$_{\text{target}}$. In this case, the process moves to Stage 2 of the methodology without going into the second iterative process.

- On the other hand, if for an iteration k we have that $k > i_{max}$, this process ends, and the second iterative process begins. Accordingly, it is concluded that the CIG_{target} cannot be reached based only on CIG operated in grid-following mode, and therefore, its penetration in the system has to be decreased.

2) SECOND ITERATIVE PROCCESS

If this second process is activated, it means that the CIG_{target} defined for the year y_{target} cannot be reached with only grid-following CIG. Hence, the penetration level of grid-following converters in the system has to be diminished. From the perspective of the generation expansion plan associated to CIG_{target}CIG$_{\text{target}}$, the process of reducing CIG implies a sort of setback in time. This way, in this step, not only the maximum level of grid-following converters is determined (Max_{CIG_gf}), but also the year from which the regulator should start demanding that new CIG units to be connected in the system are connected in grid-following+f mode. To determine the value of Max_{CIG_gf} that the system can take in this case, the iterative process shown in Fig. 6 is followed.

The process starts by diminishing the installed capacity of grid-following CIG in blocks of Δ_{CIG} [MW], which are previously defined. For this, the first units that are taken out of service are the last ones connected according to the expansion plan, prioritizing those plants located in the frequency control areas with low levels of inertia (weak areas of the grid). As in previous stages, the process continues with the parameter tuning of the CIG controllers, followed by a stability assessment. This iterative process ends when, for a given iteration,

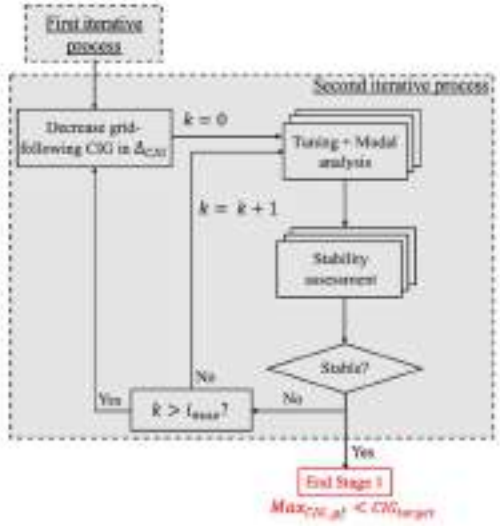

FIGURE 6. Block diagram of second iterative process of Stage 1.

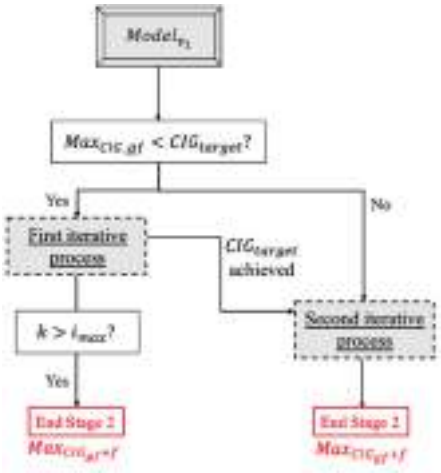

FIGURE 7. Block diagram of Stage 2.

the dynamic performance of a system complies with current regulations and is stable for all selected critical contingencies.

As a result of this stage, the maximum level of CIG able to operate in the system considering grid-following converters (Max_{CIG_gf}) is obtained. The dynamic model of the system that is obtained for the Max_{CIG_gf} penetration level is called $Model_{v1}$.

D. STAGE 2: MAXIMUM LEVEL OF CIG IN GRID-FOLLOWING+f MODE

Assuming that the system has the maximum level of grid-following converters connected already, the objective of this stage is to determine the additional CIG that can be connected in grid-following+f mode ($Max_{CIG_{gf}+f}$), so that system stability can be maintained. As in Stage 1, this is done through several iterative processes that include a tuning process followed by a stability assessment. Fig.7 shows a general scheme of Stage 2.

From the previous diagram, it can be seen that the second stage of the methodology depends on the maximum CIG level obtained in Stage 1 (CIG_{target}).

- If $Max_{CIG\_gf} < CIG_{target}$, Stage 2 begins in the first iterative process.
- If $Max_{CIG\_gf} \geq CIG_{target}$, Stage 2 starts directly in the second iterative process, without going through the first iterative process.

More details of both blocks are presented in the next section.

1) FIRST ITERATIVE PROCCESS

If $Max_{CIG\_gf} < CIG_{target}$, there are CIGs of the generation expansion plan that cannot be connected in grid-following mode in Stage 1. To be consistent with the generation roadmap associated to CIG_{target}, in this stage, those units are precisely the first ones to be incorporated in grid-following+f mode. The incorporation process is realized following the scheduling of the generation expansion plan.

As in previous stages, the process entails progressively increasing the level of CIG in grid-following+f mode, parameter tuning, including in this case, the parameters of droop loops of frequency of CIG to then assess if the power system has a good dynamic performance for said CIG level. If that is the case, the penetration of CIG is increased, and the dynamic performance is assessed once again. The performance indicators, as well as their boundary values, are the same as those used in previous stages. This process ends when, for a certain iteration k, one of the following conditions is met:

- There is no more CIG to be connected in the generation expansion plan and the system is stable for all simulated critical contingencies. In this case, we have that the target is reached through a combination of CIG units in grid-following and grid-following+f mode. Then, the process continues and goes to the second iterative process.
- For a given iteration k we have that $k > i_{max}$, the process ends and goes directly to Stage 3 of the proposed methodology (without going through the second iterative process). It is concluded, by consequence, that CIG_{target} cannot be reached based on converters in grid-following mode only, even if some of them embed additional frequency control functions.

2) SECOND ITERATIVE PROCCESS

In this stage it is assumed that the CIG_{target} has already been reached through a combination of grid-following converters with and without frequency control. In this way and from this point onward, there is no generation expansion plan to follow, and so the increase of CIG is made taking conventional SGs out of service (those that are still in operation in the year y_{target}).

The process of displacing SGs by CIGs in grid-following+f mode is done progressively, starting with those machines located near the best RES potential (solar or wind). In each iteration, a conventional power plant is replaced with a CIG of equivalent capacity to then continue with the same process of parameter tuning and stability assessment described in previous stages. The end of this iterative process can take place in the following two cases:

- When, for a given iteration k, we have that $k > i_{max}$, that is, for the CIG level considered, the dynamic performance of the system does not reach stability for all critical contingencies considered.
- When, for a given iteration k, there is only one SG to be replaced.

The restriction of keeping at least one SG connected to the system in Stage 2 is justified because a real power system cannot operate without having at least one generating unit able to participate in the process of forming frequency and voltage [7]. Further, according to [24], black-start following a power system outage could present a great challenge if grid-following CIG have replaced most SG with black-start capability.

As a result of this stage, the maximum level of CIG operating in grid-following+f mode that can be incorporated to the system ($Max_{CIG_{gf}+f} < CIG_{target}$) is obtained. The dynamic model that is obtained in this stage is called $Model_{v2}$, and it includes the $Max_{CIG\_gf}\%$ of CIG in grid-following mode and the $Max_{CIG_{gf}+f}\%$ of CIG in grid- grid-following+f mode.

E. STAGE 3: MAXIMUM LEVEL OF CIG CONSIDERING GRID-FORMING MODE

In the last stage of the methodology, the feasibility of operating the system when there are no synchronous machines in operation is studied. For this, the starting point is the grid resulting from Stage 2 ($Model_{v2}$) and the SGs still connected to the system begin to be replaced with CIG units operating in grid-forming mode. This is done following the same iterative procedure of previous stages.

As a result of Stage 3, we obtain the maximum level of CIG that can be integrated into the power system under study, considering the three types of operating modes: grid-following, grid-following+f, and grid-forming.

IV. CASE STUDY DESCRIPTION

A. INTRODUCTION

In this work, we use the Chilean power system as a case study. From a frequency stability perspective, the Chilean case is particularly interesting because it is an isolated network with an extreme longitudinal topology of 3100 kilometers long and low levels of inertia (even without CIG). These features make this system one that is inherently less robust, and hence, likely to face instabilities. Additionally, the Chilean system already has high levels of CIG concentrated in the north area of the country (Atacama Desert), which is an area that concentrates one of the most attractive solar potentials in the world. In fact, Chile has an installed capacity of 5349 MW based on CIG already, which is equivalent to 21.6% of the total installed capacity in the country [72]. Out of this capacity, 3206 MW are based on PV power plants installed in the north of the country.

For the year 2050, the Chilean government has set the goal to reach at least 70% of generation based on RES [73]. In this context, we used the system projected for the year 2046 according to official estimations by the government. The projection used is based on one of the energy scenarios contemplated in the Long-term Power Plan (similar to a generation expansion plan) elaborated by the Ministry of Energy of Chile in 2017 [74]. In this scenario, the total generation capacity installed at the national level for the year 2046 is 38236 MW, out of which 27679 MW correspond to CIG (including more PV power plants in the North and wind power plants in the south). In this way, for the year 2046 it is contemplated that 72% of the total generation capacity installed in the system will be based on CIG and only the remaining 28% (i.e., 10557 MW) based on conventional SG.

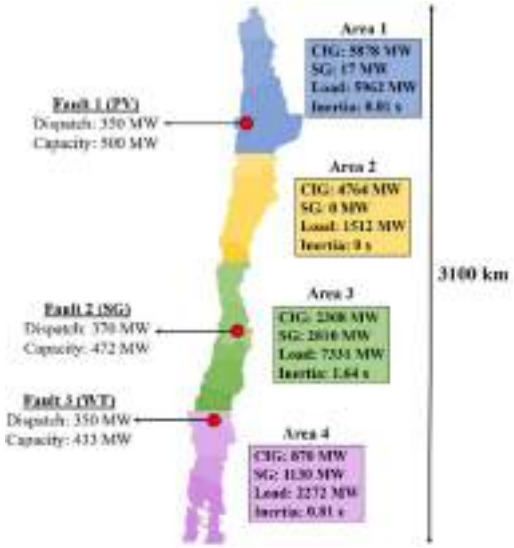

FIGURE 8. Injected power by CIG and SGs per frequency control area.

B. SYSTEM OPERATING CONDITION

Given that the focus of this work is the frequency stability in grids with high levels of CIG, the proposed methodology is applied for the minimum net load of the system projected for the year 2046. In this scenario, the total system load is 17077 MW and the total power generated is 17777 MW, out of which 13820 MW are generated by CIG. In this way, 78% of the demand is supplied by CIG-based power plants.

The system under study is shown in Fig. 8, where the colors are used only to distinguish frequency control areas. To the right of each area there is a chart that includes the demand and power generated by CIG and SG for the minimum net load operating point, along with the inertia per area (with a common base of 10557 MW). Additionally, the red dots indicate the location of the critical contingencies studied. Note that, as usual in frequency stability assessments of realistic size power systems, critical contingencies considered for the simulations are sudden outages of large online generation units [69], [75].

As seen in Fig. 8, most of the power generated in the north area of the country (areas 1 and 2) is generated by CIG, while in central and southern areas (areas 3 and 4) the power generation is distributed more evenly between CIG and SG.

C. SYSTEM DYNAMIC MODEL

The dynamic model developed for the Chilean system is a detailed model with 2400 busbars, 1560 transmission lines, and 1175 load points distributed along the grid. The model was implemented in DIgSILENT PowerFactory [76] and is based on the official model of the Chilean system available on the website of the Chilean TSO [77]. To model the existing generation plants in the system, the same dynamic models in the official TSO model were used. The loads are modeled using voltage-dependent models. The generator models correspond to the classical fifth order model with two damping windings, in which stator transients are neglected [13]. For expanding the system to the year 2046, new transmission assets and generation units are modeled considering the long-term energy planning developed by the Chilean government [74].

For modeling future wind and PV plants, we develop two models depending on the converter's operating mode:

- For converters operating in grid-following mode, we implemented dynamic models based on generic WECC models for WT and PV power plants [78], [79]. In both models, CIGs are controlled as voltage sources whose angular reference is provided by a PLL. To do this, the original WECC models were adapted to explicitly incorporate an SRF-PLL [45] in the converter control scheme. As shown in Fig. 1, both models consist of an outer active power/voltage control, an inner current controller, and the PLL that provides the angular reference to the inner control loop. Additionally, the implemented WECC models have filters for the measurement of voltage and power. The time constants for the filters are the default values of the WECC templates in DIgSILENT: for PV plants 0.02 s is used for all the measurements, whereas for WT plants 0.01 s and 0.05 s are used for the voltage and power measurements, respectively.
- For grid-forming converters, we implemented the droop-based model shown in Fig. 3, which has been widely used in the literature [2], [39], [43]. The model has an outer power/voltage control loop and an inner current control loop, whose output is the voltage to be formed at the PCC. The parameter values used are those considered in [7].

The PLL bandwidth used in the grid-following converters is 6 Hz because it represents an intermediate value between typical values considered in stability studies of large-scale power systems with high CIG penetration levels (see, for example, [7], [12], [80]–[82], in which PLL bandwidth values are within the range of 1 to 13 Hz). With these values, the PLL is capable of *correctly* following the phase of the voltage at the PCC during normal operation. Higher PLL bandwidths are not commonly used in power systems with high levels of CIG as they can significantly affect the small-signal stability of the system [63], [83]. Parameter tuning (K_{vp}, K_{vi}) of the PI in the voltage control loop is made on a trial-and-error fashion by considering typical values found in literature. Concretely, for the parameter K_{vp}, a sensibility analysis is performed using values between 0 and 5, while for K_{vi}, values in the range of 0.5 to 25 are used [52], [54], [83]–[85].

Finally, to allow frequency support capability in CIG, we consider a de-loaded operation in both grid-following+f and grid-forming converters. The droop coefficients used in both grid-forming and grid-following+f converters are $m = 5\%$ and $n = 0\%$ as they are typical values found in the literature [7], [19], [64], [65]. It is important to highlight that the choice of the droop coefficients is a techno-economical problem that should be optimized [86], [87]. Although this

TABLE 1. System dynamic performance indicators for different parameters combinations.

K_{vp} [pu]	K_{vi} [pu]	ξ_{min} [%]	f_{nadir} [Hz]	T_s [s]
1	0.7	-19.59	-	-
2	0.7	4.4	48.447	>100
3	0.7	4.5	48.459	>100
5	0.7	4.5	48.501	>100
5	2	4.5	48.618	>100
5	5	4.5	48.687	>100
5	15	4.5	48.732	>100
5	25	4.5	48.744	>100

is a highly interesting problem, it is out of the scope of this paper and is not further discussed. In addition, it is worth mentioning that, although the proposed methodology is independent of the architecture and control parameters adopted in the converters, the results obtained may be different if other dynamic models and control parameters are used.

V. OBTAINED RESULTS

In this section, the results obtained for the Chilean case projected to the year 2046 are presented after applying the proposed methodology in Section III.

A. MAXIMUM LEVEL OF CIG IN GRID-FOLLOWING MODE ONLY (BUSINESS-AS-USUAL)

As explained in Section III, the first methodological stage seeks to determine the maximum level of grid-following CIG (Max_{CIG_gf}) that can be incorporated based on two iterative processes. The first process determines if CIG_{target} can be reached only based on grid-following converters. If this is not possible, then the second iterative process is conducted. In this process, the grid-following CIG installed capacity is progressively decreased until a proper system performance is achieved. Both steps are carried out through an iterative process that includes parameter tuning followed by a stability assessment that takes into account a set of critical contingencies. Due to space constraints, the following section summarizes only the main conclusions obtained in each stage.

1) FIRST ITERATIVE PROCESS: CIG_{target} ONLY WITH GRID-FOLLOWING CIG

Table 1 summarizes how some of the system dynamic performance indicators change for different parameter combinations when the amount of grid-following CIG is equal to CIG_{target}. The indicators shown are the minimum damping (ξ_{min}) obtained from the modal analysis (related to a specific mode), as well as the frequency nadir (f_{nadir}) and settling time (T_s) when fault 1 is simulated. Even though the table shows a limited range of the values for K_{vp} and K_{vi}, the analysis included a much larger number of combinations. This table only includes the value combinations that provided the best results from a stability perspective.

From the table above, it can be observed that as the K_{vp} and K_{vi} values increase, the frequency nadir of the system

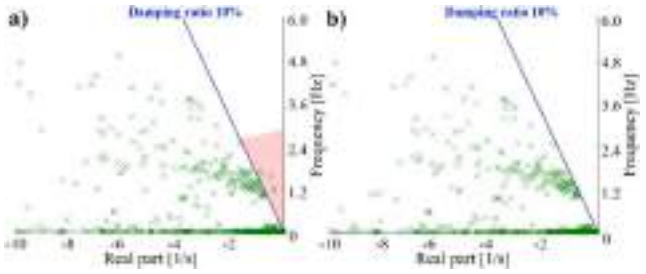

FIGURE 9. Modal analysis a) Without PSS retuning; b) retuning PSS.

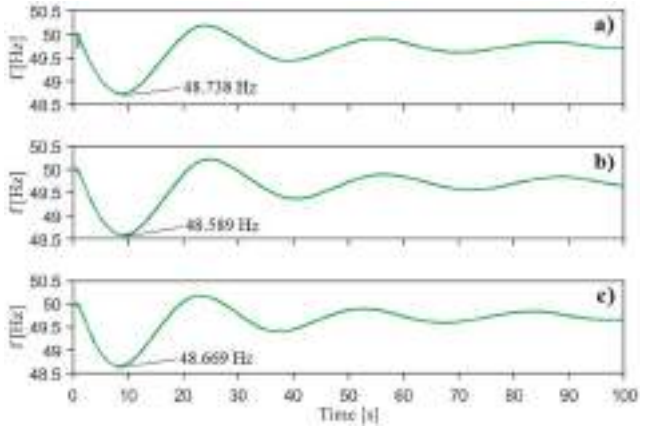

FIGURE 10. System frequency during critical contingencies considering 78% of grid-following CIG a) Fault 1, b) Fault 2, c) Fault 3.

after fault 1 improves. However, the improvement is not significant. Although not shown in the table, when K_{vi} increases to values over 25 ($K_{vi} > 25$) the improvement in the nadir becomes marginal. This may be due to the measurement filters values used in the PV and WT plants, which could restrict the values adopted for K_{vp} and K_{vi} [88]. Finally, for values $K_i \leq 1$, the system becomes unstable, which is why these results are not shown in the table above.

Even though it can be inferred from the table that the best parameter combination is $K_{vP} = 5$ and $K_{vi} = 25$, the lowest damping ratio (among all eigenvalues) does not comply with the minimum damping of 10% established in the Chilean grid code. Additionally, the frequency nadir after fault 1 is lower than 49 Hz ($f_{nadir} = 48.744$ Hz, $f_{nadir} = 48.744 f_{nadir} = 48.744$), which in the Chilean case, implies the activation of under frequency load shedding schemes (UFLSS). In light of this, the tuning process is conducted once again, but this time by considering the PSS of some key generators in the system. Fig. 9 shows the eigenvalues of the system when $K_P = 5$ and $K_i = 25$ with and without PSS retuning. The axes of both graphs have been reduced to show the window of electromechanical modes. The red-colored area indicates the oscillation modes with damping ratio lower than 10%.

As shown in Fig. 9, the retuning of some key PSS contributes to increase the damping ratio of the modes that were initially not correctly damped (ξ <10%). However, the frequency of the system continues to fall below 49 Hz

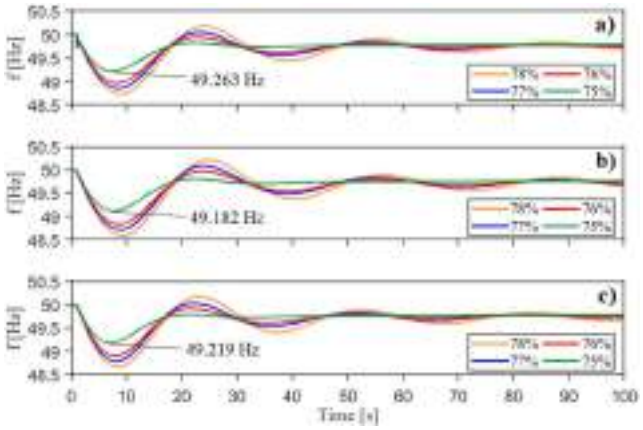

FIGURE 11. System frequency during critical contingencies for different levels of grid-following CIG a) Fault 1, b) Fault 2, c) Fault 3.

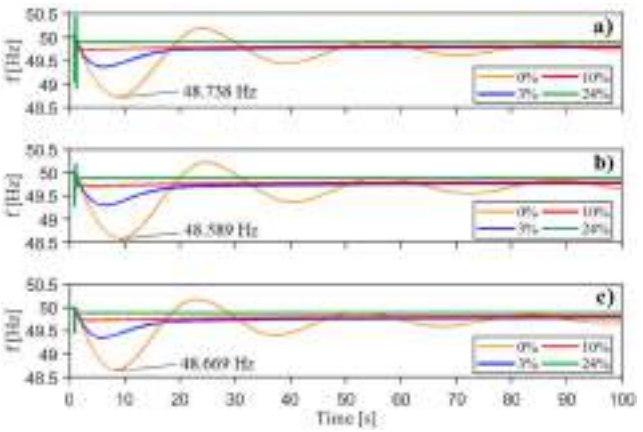

FIGURE 12. System frequency during critical contingencies for different levels of grid-following+f CIG a) Fault 1, b) Fault 2, c) Fault 3.

during extreme contingencies, which implies a loss of energy supply. The frequency evolution in a representative busbar of the grid during faults 1, 2 and 3 (applied in $t = 1$ s) is presented in Fig. 10. It is observed that the post-fault frequency oscillations do not have a good damping level. In fact, at 100 seconds, the frequency does not yet manage to stabilize in its steady-state value.

The previous iterative process (parameter tuning followed by a dynamic assessment) was conducted for a total of i_{max} iterations without reaching satisfying results in terms of the minimum performance required for the indicators. According to the proposed methodology, it is concluded that the CIG_{target} cannot be reached using only CIG operated in grid-following mode. Hence, the penetration of grid-following CIG in the system has to be decreased.

2) SECOND ITERATIVE PROCCESS: REDUCTION OF GRID-FOLLOWING CIG

In the second iterative process of Stage 1, the level of grid-following CIG in the system is progressively decreased until reaching the maximum level that complies with the minimum performance of the indicators. For this, we first took grid-following CIG plants out of service, according to the expansion plan (the first units to be taken out of service are the last ones to be connected to the system according to the expansion plan) by prioritizing those plants located in frequency control areas with low levels of inertia. This step-by-step iterative process was explained in detail in Section III; only the obtained results will be presented.

Once the second iterative process was conducted, we have that four grid-following CIG power plants with a total installed capacity of 730 MW should be taken out of service. In Fig. 11, the behavior of system frequency for the critical contingencies is presented. Each graph presents the frequency evolution in 4 iterations of the process, that is, for different levels of grid-following CIG connected to the system: (i) 78%, (ii) 77%, (iii) 76%, and (iv) 75%.

As expected, the frequency performance improves as the penetration of grid-following converters decreases. This improvement is reflected both in the frequency nadir of the system and the damping of post-fault frequency oscillations. This can be explained due to the fact that the CIG reduction comes with an increase of conventional synchronous generation, which are units that contribute to both inertial response and primary frequency control of the system. Fig. 11 shows that, when the level of grid-following CIG equals 75%, the system frequency nadir reaches values over 49 Hz for all selected critical contingencies, thus complying with the established performance indicators. Based on these results, we conclude that the maximum level of grid-following CIG for the case under study is 75%, that is, $Max_{CIG\_gf} = 75\%$.

B. STAGE 2: MAXIMUM LEVEL OF CIG IN GRID-FOLLOWING+f MODE

The objective of this stage is to determine the additional CIG that can be connected to the system in grid-following+f mode (i.e., CIG with frequency droop controllers) as a way to maintain power system stability. For this, we start by assuming that the power system already has a grid-following CIG penetration $Max_{CIG\_gf} = 75\%$. As in Stage 1, this step is conducted based on several iterative processes that include a tuning process followed by a stability assessment.

As explained in Section III, since $Max_{CIG\_gf} < CIG_{target}$, the first units that are added to the system in grid-following+f mode are the same CIG from the generation roadmap that were taken out of service in the previous stage.

Once CIG_{target} is reached, we proceed to iteratively replace conventional machines with grid-following+f CIG, according to the prioritization detailed in Section III. Fig. 12 shows the frequency behavior for the three critical faults. Each graph presents the frequency evolution considering different levels of grid-following+f CIG connected to the system (in this case, in 4 iterations): (i) 0%, (ii) 3%, (iii) 10%, and (iv) 24%. In iterations (ii), (iii), and (iv), SGs were progressively displaced in areas 1, 4, and 3, respectively (considering the inertia values registered in Fig. 8).

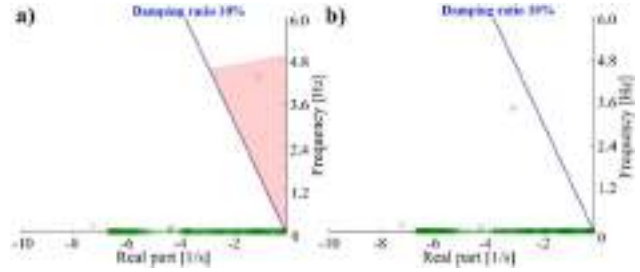

FIGURE 13. Modal analysis in 100% based CIG power system (75% grid-following and 25% grid-following+f) a) Without retuning PLLs; b) retuning PLLs.

This figure shows that as the CIG levels increase by means of frequency droop controllers, the frequency behavior improves considerably. Even for the case in which the level of grid-following+f is only 3%, frequency already complies with the minimum performance requirements established by Chilean technical regulations. Concretely, the nadir is higher than 49.3 Hz and the settling time is less than 40 s for the 3 critical contingencies. It is important to observe that as the CIG participation increases, system frequency acquires a much faster dynamic in comparison to what is observed in conventional systems. In fact, when the level of grid-following+f is 10%, the frequency stabilizes in its steady state value after approximately 15 s, whereas when the level of grid-following+f is 24%, it is stabilized in less than 5 s. This settling time is considerably shorter than that observed in the simulations previously presented and, in general, shorter than typical settling times in conventional systems dominated by SG.

Therefore, the system can operate with a level of grid-following+f equal to 24% ($Max_{CIG_{gf}+f} = 24\%$), which in this case implies that only one SG is in operation by contributing 1% of the total load of the system.

C. STAGE 3: MAXIMUM LEVEL OF CIG CONSIDERING GRID-FORMING MODE

From the results obtained in the previous stage, in this stage the only SG in service is replaced with a CIG plant. For comparison purposes, two cases are considered for this analysis: 1) SG replaced with a grid-following+f converter, and 2) SG replaced with a grid-forming converter.

1) LAST ONLINE SG REPLACED WITH A GRID-FOLLOWING+f CONVERTER

When replacing the last SG in service by a grid-following+f converter, the modal analysis yields only stable modes. However, as shown in Fig. 13, there is a pair of eigenvalues not well damped, with a damping ratio of $\xi = 3.85\%$. Accordingly, the minimum established damping requirement of 10% is not met. The oscillation frequency of this mode is 4.4 Hz, and according to the participation factors, it is associated with a state variable of the PLL of some of the CIG power plants with larger capacity.

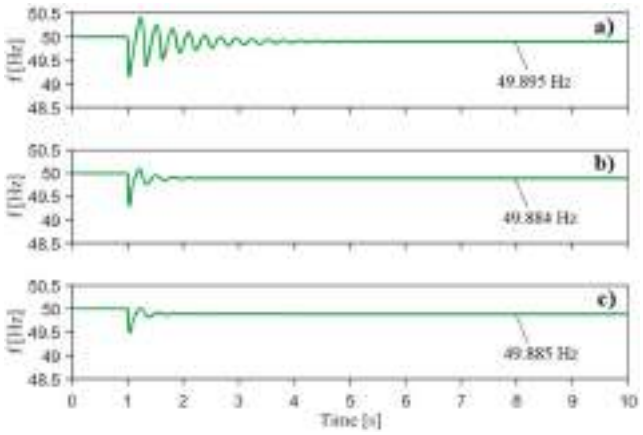

FIGURE 14. System frequency during critical contingencies in 100% based CIG power system (75% grid-following and 25% grid-following+f) a) Fault 1, b) Fault 2, c) Fault 3.

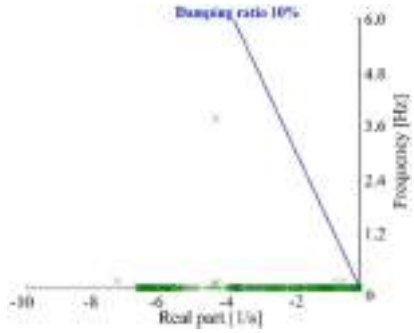

FIGURE 15. Modal analysis in 100% based CIG power system (75% grid-following, 24% grid-following+*f, and 1% grid-forming*).

To increase the damping of these modes, the PLL gains (K_P, K_i) of the grid-following+f converters that replaced SGs are retuned. Concretely, PLL gains ($K_{P_{PLL}}, K_{i_{PLL}}$) are reduced to decrease the PLL bandwidth from 6 Hz to 3 Hz and hence improve the small-signal behavior of the system. In fact, some studies have shown that in weak grids with high levels of CIG, PLLs with high bandwidth values can compromise the small-signal stability [42], [69], [74]. The results of this retuning are shown in Fig. 13 (b), where it can be observed that there are no poorly-damped modes. It is interesting to observe that in Fig. 13 (b), the electromechanical oscillation modes that are usually observed in SG-dominated systems do not appear. This becomes evident when comparing the results of Fig. 13 (b) with those presented in Fig. 9.

Once the PLL retuning is conducted, the critical faults are simulated (sudden disconnections of generation at t = 1 s). Fig. 14 depicts the system frequency evolution in a representative busbar of the grid during faults 1, 2, and 3.

From Fig.14 it can be observed that the system remains stable after the 3 critical faults and that the frequency nadir is higher than 49 Hz in all cases. As in the scenario in which there was only one SG (Fig. 12), after the contingency, the system frequency presents some oscillations that are rapidly damped so that it reaches its steady-state value in less than 5 s.

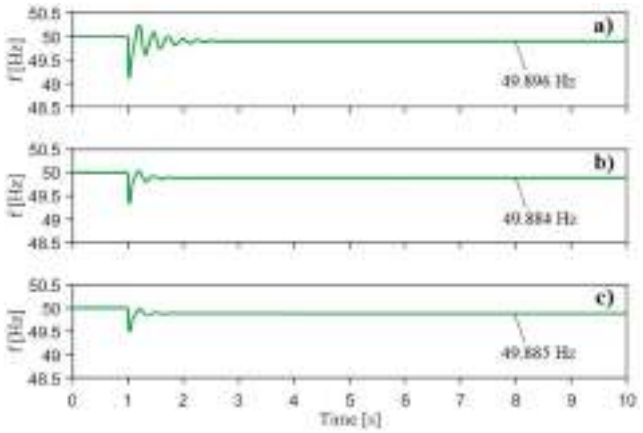

FIGURE 16. System frequency during critical contingencies in 100% based CIG power system (75% grid-following, 24% grid-following+*f, and 1% grid-forming)* a) Fault 1, b) Fault 2, c) Fault 3.

TABLE 2. Results summary for different faults and CIG penetration scenarios.

Scenario	H [s]	Fault	f_{nadir} [Hz]	T_{nadir} [s]	T_s [s]
78% GFL 22% SG	2.46	1	48.74	7.86	74.08
		2	48.59	8.25	77.64
		3	48.67	7.48	71.73
75% GFL 25% SG	2.91	1	49.26	6.43	15.11
		2	49.18	6.71	15.64
		3	49.22	6.12	14.82
75% GFL 3% GFL+f 22% SG	2.46	1	49.37	5.23	16.03
		2	49.30	5.44	16.78
		3	49.35	4.96	15.57
75% GFL 24% GFL+f 1% SG	0.08	1	48.92	0.29	0.39
		2	49.29	0.07	0.36
		3	49.45	0.08	0.27
75% GFL 25% GFL+f	0	1	49.11	0.07	1.57
		2	49.32	0.07	0.38
		3	49.46	0.07	0.28
75% GFL 24% GFL+f 1% GFM	0	1	49.13	0.07	0.62
		2	49.36	0.07	0.25
		3	49.48	0.06	0.11

Although Fig. 14 (a) shows that in the case of fault 1 oscillations have a higher amplitude and duration in comparison to faults 2 and 3, this is explained because fault 1 is located in an area with a large amount of CIG.

2) LAST ONLINE SG REPLACED WITH A GRID-FORMING CONVERTER

Finally, the behavior of the system is verified when the last SG in service is replaced with a grid-forming converter. As illustrated in Fig. 15, in this case, the modal analysis does not yield poorly damped modes ($\xi < 10\%$), thus it is not necessary to conduct a retuning of the CIG controllers. The figure shows that there are no electromechanical oscillation modes associated with synchronous machines.

The system frequency during the simulated critical faults is presented in Fig. 16. From the figure it can be seen that in this case, the system is also stable during and after the 3 faults. Additionally, and as in Fig. 14, the frequency shows very fast dynamics with settling times between 1 and 3 seconds. Finally, it is worth mentioning that for the 3 critical faults, the system frequency performance improves when incorporating a grid-forming CIG in comparison to the results obtained in Fig. 14 (only with grid-following and grid-following+f CIG), especially in fault 1.

D. RESULTS SUMMARY

Table 2 summarizes the results obtained for the most relevant simulated scenarios. The nomenclature used in the table is based on synchronous generation (SG), grid-following (GFL), grid-following+f (GFL +f), grid-forming (GFM), and total system inertia (H). The performance indicators registered are the frequency nadir (f_{nadir}), the time to reach the frequency nadir (T_{nadir}), and the frequency stabilization time (T_s), which is defined as the time required for the frequency to reach and remain within a band of ± 0.1 Hz around its final value.

From Table 2 it can be seen that, due to the fast response of CIGs, T_{nadir} and T_s are reduced as the penetration of CIG with frequency controllers increase.

VI. CONCLUSION

This article presents a novel methodology for systematically determining the control requirements to impose on CIG-based power plants as their penetration in the network increases. Although the proposed methodology is especially designed for ensuring frequency stability, it can be applied considering other types of stability as long as some minor changes are undertaken such as the kind of contingency to be simulated and the definition of the control areas.

The methodology allows to systematically determine (i) the maximum level of grid-following CIG, (ii) the penetration level from which grid-following CIG should be required to embed frequency control capability and (iii) the point from which CIG should operate in grid-forming mode to contribute to the process of forming frequency and voltage.

Results of a case study based on a detailed dynamic model of the Chilean grid projected for the year 2046 allowed us to draw several major conclusions. First, the maximum level of CIG penetration considering only the most basic form of grid-following converters (without frequency control capability) is 75%, which is below the Chilean target of 78% CIG penetration for the year 2046. To achieve the Chilean target, 3% should be based on grid-following CIG with frequency controllers to provide frequency support. Moreover, our results show that further incorporation of grid-following CIGs with frequency control capability can reach 99% CIG penetration where only one SG remains in operation. Finally, we showed that replacing the last online SG with a grid-forming converter (thus achieving a 100% based CIG system) is also technically possible from a frequency stability viewpoint.

The proposed methodology represents a first attempt to systematically define the control requirements to be imposed on CIG to ensure frequency stability as its penetration in power systems increases. From the economic viewpoint, said methodology can also be used by system operators or

energy regulators as a support tool in the design of grid code requirements related to frequency control capability in CIGs. To comply with any kind of frequency control obligation, CIG must be either operated in de-loaded mode or incorporate an energy storage system, requiring this capability without a proper technical justification may significantly hinder the deployment of CIG.

In future work, the proposed methodology will be extended to include the requirements related to other types of stability, namely, voltage, converter-driven, electric resonance, and rotor angle stability. Only by considering all dynamic phenomena will we be able to accurately determine the converters' control requirements that ensure the stable operation of power systems dominated by CIG.

ACKNOWLEDGMENT

The authors would like to thank Elliott Fix at Temple University for his valuable contribution to this paper.

REFERENCES

[1] B. Kroposki, B. Johnson, Y. Zhang, V. Gevorgian, P. Denholm, B.-M. Hodge, and B. Hannegan, "Achieving a 100% renewable grid: Operating electric power systems with extremely high levels of variable renewable energy," *IEEE Power Energy Mag.*, vol. 15, no. 2, pp. 61–73, Mar. 2017.

[2] F. Milano, F. Dorfler, G. Hug, D. J. Hill, and G. Verbic, "Foundations and challenges of low-inertia systems (invited paper)," in *Proc. Power Syst. Comput. Conf. (PSCC)*, Jun. 2018, pp. 1–25.

[3] IRENA. (2020). *Renewable Capacity Statistics 2020*. Accessed: Mar. 15, 2021. [Online]. Available: https://irena.org/publications/2020/Mar/Renewable-Capacity-Statistics-2020

[4] IRENA. (2021). *Renewable Capacity Statistics 2021*. Accessed: Apr. 27, 2021. [Online]. Available: https://www.irena.org/publications/2021/March/Renewable-Capacity-Statistics-2021

[5] J. Lee and F. Zhao, "GWEC global wind report 2019," *Wind Energy Technol.*, pp. 1–78, Mar. 2020. Accessed: Mar. 10, 2021. [Online]. Available: https://gwec.net/wp-content/uploads/2020/08/Annual-Wind-Report_2019_digital_final_2r.pdf

[6] *Snapshot of Global PV Markets 2020*, Int. Energy Agency, Paris, France, 2020, pp. 1–16. Accessed: Mar. 12, 2021. [Online]. Available: https://iea-pvps.org/wp-content/uploads/2020/04/IEA_PVPS_Snapshot_2020.pdf

[7] X. Zhao, P. Guhathakurta, and D. Flynn. (2019). *New Options in System Operations*. Accessed: Feb. 18, 2021. [Online]. Available: https://www.h2020-migrate.eu/_Resources/Persistent/5d0f8339650bcf53cd24a3006556daa1da66cb42/D3.4%20-%20New%20Options%20in%20System%20Operations.pdf

[8] S. A. Ballesteros and D. W. Martin. (2013). *Meeting Renewable Energy Targets: Global Lessons From the Road to Implementation*. [Online]. Available: http://awsassets.panda.org/downloads/meeting_renewable_energy_targets__low_res_.pdf.

[9] N. Hatziargyriou, J. Milanović, C. Rahmann, V. Ajjarapu, C. Cañizares, I. Erlich, D. Hill, I. Hiskens, I. Kamwa, B. Pal, P. Pourbeik, J. Sánchez-Gasca, A. Stanković, T. Van Cutsem, V. Vittal, and C. Vournas, "Stability definitions and characterization of dynamic behavior in systems with high penetration of power electronic interfaced technologies," IEEE Power Energy Soc., Tech. Rep. PES-TR77, Apr. 2020, pp. 1–42.

[10] C. Rahmann, V. Vittal, J. Ascui, and J. Haas, "Mitigation control against partial shading effects in large-scale PV power plants," *IEEE Trans. Sustain. Energy*, vol. 7, no. 1, pp. 173–180, Jan. 2016.

[11] M. Paolone, T. Gaunt, X. Guillaud, M. Liserre, S. Meliopoulos, A. Monti, T. Van Cutsem, V. Vittal, and C. Vournas, "Fundamentals of power systems modelling in the presence of converter-interfaced generation," *Electr. Power Syst. Res.*, vol. 189, Dec. 2020, Art. no. 106811.

[12] D. Ramasubramanian, E. Farantatos, S. Ziaeinejad, and A. Mehrizi-Sani, "Operation paradigm of an all converter interfaced generation bulk power system," *IET Gener., Transmiss. Distrib.*, vol. 12, no. 19, pp. 4240–4248, Oct. 2018.

[13] J. Vega-Herrera, C. A. Rahmann, F. Valencia, and K. Strunz, "Analysis and application of quasi-static and dynamic phasor calculus for stability assessment of integrated power electric and electronic systems," *IEEE Trans. Power Syst.*, vol. 36, no. 3, pp. 1750–1760, May 2021.

[14] A. Ulbig, T. S. Borsche, and G. Andersson, "Impact of low rotational inertia on power system stability and operation," *IFAC Proc. Volumes*, vol. 47, no. 3, pp. 7290–7297, 2014.

[15] NERC. (Jun. 2017). *Integrating Inverter Based Resources Into Weak Power Systems Reliability Guideline*. Accessed: Mar. 27, 2021. [Online]. Available: https://www.nerc.com/comm/RSTC_Reliability_Guidelines/Item_4a._Integrating%20_Inverter-Based_Resources_into_Low_Short_Circuit_Strength_Systems_-_2017-11-08-FINAL.pdf#search=Integrating%20Inverter%20Based%20Resources%20into%20Weak%20Power%20Systems%20Reliability%20Guideline

[16] J. Adams, C. Carter, and S. H. Huang, "ERCOT experience with sub-synchronous control interaction and proposed remediation," in *Proc. PES T&D*, Orlando, FL, USA, 2012, pp. 1–5.

[17] P. Tielens and D. Van Hertem, "The relevance of inertia in power systems," *Renew. Sustain. Energy Rev.*, vol. 55, pp. 999–1009, Mar. 2016.

[18] I. Erlich, A. Korai, and F. Shewarega, "Control challenges in power systems dominated by converter interfaced generation and transmission technologies," in *Proc. IEEE Power Energy Soc. Gen. Meeting*, Sep. 2017, pp. 1–5.

[19] U. Markovic, "Towards reliable operation of converter-dominated power systems: Dynamics, optimization and control," Ph.D. dissertation, ETH Zürich Univ., Zürich, Switzerland, 2020.

[20] D. Groß and F. Dörfler, "On the steady-state behavior of low-inertia power systems," *IFAC-PapersOnLine*, vol. 50, no. 1, pp. 10735–10741, 2017.

[21] G. Delille, B. François, and G. Malarange, "Dynamic frequency control support by energy storage to reduce the impact of wind and solar generation on isolated power system's inertia," *IEEE Trans. Sustain. Energy*, vol. 3, no. 4, pp. 931–939, Oct. 2012.

[22] C. Rahmann and A. Castillo, "Fast frequency response capability of photovoltaic power plants: The necessity of new grid requirements and definitions," *Energies*, vol. 7, no. 10, pp. 6306–6322, Oct. 2014.

[23] M. Dreidy, H. Mokhlis, and S. Mekhilef, "Inertia response and frequency control techniques for renewable energy sources: A review," *Renew. Sustain. Energy Rev.*, vol. 69, pp. 144–155, Mar. 2017.

[24] Y. Lin, J. Eto, B. Johnson, J. Flicker, R. Lasseter, H. Villegas, G. Seo, B. Pierre, and A. Ellis. (2020). *Research Roadmap on Grid-Forming Inverters*. Accessed: Mar. 26, 2021. [Online]. Available: https://www.nrel.gov/docs/fy21osti/73476.pdf

[25] U. Markovic, O. Stanojev, P. Aristidou, and G. Hug, "Partial grid forming concept for 100% inverter-based transmission systems," in *Proc. IEEE Power Energy Soc. Gen. Meeting (PESGM)*, Aug. 2018, pp. 1–5.

[26] J. Rocabert, A. Luna, F. Blaabjerg, and P. Rodriguez, "Control of power converters in AC microgrids," *IEEE Trans. Power Electron.*, vol. 27, no. 11, pp. 4734–4749, Nov. 2012.

[27] X. Wang, J. M. Guerrero, F. Blaabjerg, and Z. Chen, "A review of power electronics based microgrids," *Int. J. Power Electron.*, vol. 12, no. 1, pp. 181–192, 2012.

[28] European Union (EU). (2016). *Commission Regulation (EU) 2016/631 of 14 April 2016 Establishing a Network Code on Requirements for Grid Connection of Generators (Text With EEA Relevance)*. Accessed: Jan. 4, 2022. [Online]. Available: http://data.europa.eu/eli/reg/2016/631/oj

[29] National Energy Regulator of South Africa (NERSA). (2019). *Grid Connection Code for Renewable Power Plants (RPPs) Connected to the Electricity Transmission System (TS) or the Distribution System (DS) in South Africa*. Accessed: Jan. 4, 2022. [Online]. Available: http://nersa.org.za/wp-content/uploads/bsk-pdf-manager/2020/09/Grid-Connection-Code-for-Renewable-Power-Plants-RPPs.pdf

[30] *IEEE Draft Standard for Interconnection and Interoperability of Inverter-Based Resources (IBR) Interconnecting With Associated Transmission Electric Power Systems*, document P2800/D6.3, IEEE Standards Association, Dec. 2021, pp. 1–181.

[31] J. Matevosyan, B. Badrzadeh, T. Prevost, E. Quitmann, D. Ramasubramanian, H. Urdal, S. Achilles, J. MacDowell, S. H. Huang, V. Vittal, J. O'Sullivan, and R. Quint, "Grid-forming inverters: Are they the key for high renewable penetration?" *IEEE Power Energy Mag.*, vol. 17, no. 6, pp. 89–98, Nov./Dec. 2019.

[32] A. Tayyebi, D. Groß, A. Anta, F. Kupzog, and F. Dörfler, "Frequency stability of synchronous machines and grid-forming power converters," *IEEE J. Emerg. Sel. Topics Power Electron.*, vol. 8, no. 2, pp. 1004–1018, Jun. 2020.

[33] B. K. Poolla, D. Groß, and F. Dörfler, "Placement and implementation of grid-forming and grid-following virtual inertia and fast frequency response," *IEEE Trans. Power Syst.*, vol. 34, no. 4, pp. 3035–3046, Jul. 2019.

[34] A. Crivellaro, A. Tayyebi, C. Gavriluta, D. Groß, A. Anta, F. Kupzog, and F. Dörfler, "Beyond low-inertia systems: Massive integration of grid-forming power converters in transmission grids," in *Proc. IEEE Power Energy Soc. Gen. Meeting*, Aug. 2020, pp. 2–6.

[35] J. Taouba, M. Uros, and G. Dominic. (2018). *New Options for Existing System Services and Needs for New System Services*. Accessed: Feb. 21, 2021. [Online]. Available: https://www.h2020-migrate.eu/_Resources/Persistent/5c5beff0d5bef78799253aae9b19f50a9cb6eb9f/D3.2 - Local control and simulation tools for large transmission systems.pdf

[36] *The MIGRATE Project*. Accessed: Mar. 2, 2021. [Online]. Available: https://www.h2020-migrate.eu/

[37] D. Ramasubramanian, V. Vittal, and J. M. Undrill, "Transient stability analysis of an all converter interfaced generation WECC system," in *Proc. Power Syst. Comput. Conf. (PSCC)*, Jun. 2016, pp. 1–7.

[38] R. Majumder, B. Chaudhuri, A. Ghosh, R. Majumder, G. Ledwich, and F. Zare, "Improvement of stability and load sharing in an autonomous microgrid using supplementary droop control loop," *IEEE Trans. Power Syst.*, vol. 25, no. 2, pp. 796–808, May 2010.

[39] T. Qoria, T. Prevost, G. Denis, F. Gruson, F. Colas, and X. Guillaud, "Power converters classification and characterization in power transmission systems," in *Proc. 21st Eur. Conf. Power Electron. Appl. (EPE ECCE Europe)*, Sep. 2019, pp. P.1–P.9.

[40] D. Ramasubramanian, Z. Yu, R. Ayyanar, V. Vittal, and J. Undrill, "Converter model for representing converter interfaced generation in large scale grid simulations," *IEEE Trans. Power Syst.*, vol. 32, no. 1, pp. 765–773, Jan. 2017.

[41] L. Fan and Z. Miao, "Wind in weak grids: 4 Hz or 30 Hz oscillations?" *IEEE Trans. Power Syst.*, vol. 33, no. 5, pp. 5803–5804, Sep. 2018.

[42] P. Pourbeik, J. J. Sanchez-Gasca, J. Senthil, J. D. Weber, P. S. Zadehkhost, Y. Kazachkov, S. Tacke, J. Wen, and A. Ellis, "Generic dynamic models for modeling wind power plants and other renewable technologies in large-scale power system studies," *IEEE Trans. Energy Convers.*, vol. 32, no. 3, pp. 1108–1116, Sep. 2016.

[43] L. Fan, *Control and Dynamics in Power Systems and Microgrids*, 1st ed. New York, NY, USA: CRC Press, 2017.

[44] R. Teodorescu, M. Liserre, and P. Rodríguez, *Grid Converters for Photovoltaic and Wind Power Systems*, vol. 29, 1st ed. London, U.K.: Wiley, 2011.

[45] S. Golestan, J. M. Guerrero, and J. C. Vasquez, "Three-phase PLLs: A review of recent advances," *IEEE Trans. Power Electron.*, vol. 32, no. 3, pp. 1894–1907, Mar. 2017.

[46] M. Karimi-Ghartemani, S. A. Khajehoddin, P. K. Jain, and A. Bakhshai, "Problems of startup and phase jumps in PLL systems," *IEEE Trans. Power Electron.*, vol. 27, no. 4, pp. 1830–1838, Apr. 2012.

[47] P. Rodriguez, J. Pou, J. Bergas, J. I. Candela, R. P. Burgos, and D. Boroyevich, "Decoupled double synchronous reference frame PLL for power converters control," *IEEE Trans. Power Electron.*, vol. 22, no. 2, pp. 584–592, Mar. 2007.

[48] S. Golestan, M. Monfared, and F. D. Freijedo, "Design-oriented study of advanced synchronous reference frame phase-locked loops," *IEEE Trans. Power Electron.*, vol. 28, no. 2, pp. 765–778, Feb. 2013.

[49] N. R. N. Ama, F. O. Martinz, L. Matakas, Jr., and F. Kassab, "Phase-locked loop based on selective harmonics elimination for utility applications," *IEEE Trans. Power Electron.*, vol. 28, no. 1, pp. 144–153, Jan. 2013.

[50] A. Bagheri, M. Mardaneh, A. Rajaei, and A. Rahideh, "Detection of grid voltage fundamental and harmonic components using Kalman filter and generalized averaging method," *IEEE Trans. Power Electron.*, vol. 31, no. 2, pp. 1064–1073, Feb. 2016.

[51] M. S. Pádua, S. M. Deckmann, G. S. Sperandio, F. P. Marafão, and D. Colón, "Comparative analysis of synchronization algorithms based on PLL, RDFT and Kalman filter," in *Proc. IEEE Int. Symp. Ind. Electron.*, Jun. 2007, pp. 964–970.

[52] L. Huang, H. Xin, Z. Li, P. Ju, H. Yuan, Z. Lan, and Z. Wang, "Grid-synchronization stability analysis and loop shaping for PLL-based power converters with different reactive power control," *IEEE Trans. Smart Grid*, vol. 11, no. 1, pp. 501–516, Jan. 2020.

[53] A. Alsaif, Z. Miao, and L. Fan, "Comparison of islanding and synchronization for a microgrid with different converter control," in *Proc. North Amer. Power Symp. (NAPS)*, Oct. 2019, pp. 1–6.

[54] L. Fan, "Modeling type-4 wind in weak grids," *IEEE Trans. Sustain. Energy*, vol. 10, no. 2, pp. 853–864, Apr. 2019.

[55] W. Liu, G. Geng, Q. Jiang, H. Fan, and J. Yu, "Model-free fast frequency control support with energy storage system," *IEEE Trans. Power Syst.*, vol. 35, no. 4, pp. 3078–3086, Jul. 2020.

[56] S. D'Arco, J. A. Suul, and O. B. Fosso, "A virtual synchronous machine implementation for distributed control of power converters in smartgrids," *Electr. Power Syst. Res.*, vol. 122, pp. 180–197, May 2015.

[57] Q.-C. Zhong and G. Weiss, "Synchronverters: Inverters that mimic synchronous generators," *IEEE Trans. Ind. Electron.*, vol. 58, no. 4, pp. 1259–1267, Apr. 2011.

[58] B. B. Johnson, M. Sinha, N. G. Ainsworth, F. Dörfler, and S. V. Dhople, "Synthesizing virtual oscillators to control islanded inverters," *IEEE Trans. Power Electron.*, vol. 31, no. 8, pp. 6002–6015, Aug. 2016.

[59] B. B. Johnson, S. V. Dhople, A. O. Hamadeh, and P. T. Krein, "Synchronization of parallel single-phase inverters with virtual oscillator control," *IEEE Trans. Power Electron.*, vol. 29, no. 11, pp. 6124–6138, Dec. 2014.

[60] C. Arghir, T. Jouini, and F. Dörfler, "Grid-forming control for power converters based on matching of synchronous machines," *Automatica*, vol. 95, pp. 273–282, Sep. 2018.

[61] B. Johnson, M. Rodriguez, M. Sinha, and S. Dhople, "Comparison of virtual oscillator and droop control," in *Proc. IEEE 18th Workshop Control Modeling Power Electron. (COMPEL)*, Jul. 2017, pp. 1–6.

[62] T. Qoria, Q. Cossart, C. Li, X. Guillaud, F. Colas, F. Gruson, and X. Kestelyn, "Local control and simulation tools for large transmission systems," MIGRATE-Eur. Commission, Brussels, Belgium, Dec. 2018, pp. 1–89. Accessed: Feb. 20, 2021. [Online]. Available: https://www.h2020-migrate.eu/_Resources/Persistent/5c5beff0d5bef78799253aae9b19f50a9cb6eb9f/D3.2 - Local control and simulation tools for large transmission systems.pdf

[63] X. Wang, M. G. Taul, H. Wu, Y. Liao, F. Blaabjerg, and L. Harnefors, "Grid-synchronization stability of converter-based resources—An overview," *IEEE Open J. Ind. Appl.*, vol. 1, pp. 115–134, 2020.

[64] A. Tayyebi, D. Groß, A. Anta, F. Kupzog, and F. Dörfler, "Interactions of grid-forming power converters and synchronous machines," 2019, *arXiv:1902.10750*.

[65] T. Qoria, "Grid-forming control to achieve a 100% power electronics interfaced power transmission systems," Ph.D. dissertation, Ecole Nationale Supérieure d'Arts et Métiers, HESAM Univ., Lille, France 2020.

[66] T. S. Borsche, T. Liu, and D. J. Hill, "Effects of rotational inertia on power system damping and frequency transients," in *Proc. 54th IEEE Conf. Decis. Control (CDC)*, Dec. 2015, pp. 5940–5946.

[67] B. K. Poolla, S. Bolognani, and F. Dörfler, "Optimal placement of virtual inertia in power grids," *IEEE Trans. Autom. Control*, vol. 62, no. 12, pp. 6209–6220, Dec. 2017.

[68] D. Gross, S. Bolognani, B. K. Poolla, and F. Dörfler, "Increasing the resilience of low-inertia power systems by virtual inertia and damping," in *Proc. IREP Bulk Power Syst. Dyn. Control Symp.*, 2017, pp. 1–13. [Online]. Available: http://control.ee.ethz.ch/~bsaverio/papers/Gross_IREP_2017.pdf

[69] D. Ortiz-Villalba, C. Rahmann, R. Alvarez, C. A. Canizares, and C. Strunck, "Practical framework for frequency stability studies in power systems with renewable energy sources," *IEEE Access*, vol. 8, pp. 202286–202297, 2020.

[70] C. Rahmann, D. Ortiz-Villalba, R. Alvarez, and M. Salles, "Methodology for selecting operating points and contingencies for frequency stability studies," in *Proc. IEEE Power Energy Soc. Gen. Meeting*, Jul. 2017, pp. 1–5.

[71] Comisión Nacional de Energía (CNE). (2020). *Norma Técnica de Seguridad y Calidad de Servicio*. Accessed: Feb. 21, 2021. [Online]. Available: https://www.cne.cl/wp-content/uploads/2020/09/NTSyCS-Sept20.pdf

[72] Energía Abierta. *Capacidad Instalada*. Accessed: Feb. 19, 2021. [Online]. Available: http://energiaabierta.cl/visualizaciones/capacidad-instalada/

[73] Ministerio de Energía Gobierno de Chile. (2014). *Energía 2050 Política Energética de Chile*. Accessed: Feb. 21, 2021. [Online]. Available: http://eae.mma.gob.cl/uploads/D03_Politica_Energetica_de__Chile_2050_Anteproyecto2.pdf

[74] Ministerio de Energía. *Planificación Energética de Largo Plazo—Escenarios Energéticos*. Accessed: Feb. 17, 2021. [Online]. Available: https://energia.gob.cl/planificacion-energetica-de-largo-plazo-escenarios-energeticos

[75] Q. Wang, J.-P. Watson, and Y. Guan, "Two-stage robust optimization for N-k contingency-constrained unit commitment," *IEEE Trans. Power Syst.*, vol. 28, no. 3, pp. 2366–2375, Aug. 2013.
[76] *DIgSILENT PowerFactory*. Accessed: Apr. 28, 2021. [Online]. Available: https://www.digsilent.de/en/powerfactory.html
[77] Coordinador Eléctrico Nacional. *Base de Datos*. Accessed: Feb. 22, 2021. [Online]. Available: https://www.coordinador.cl/desarrollo/documentos/estudios-de-planificacion/estudio-de-operacion-y-desarrollo-del-sen-sin-centrales-a-carbon/base-datos-estudio-operacion-y-desarrollo-sen-sin-centrales-a-carbon/
[78] *Central Station Photovoltaic Power Plant Model Validation Guideline*, Western Electr. Coordinating Council, Salt Lake City, UT, USA, 2015.
[79] P. Pourbik, "Specification of the second generation generic models for wind turbine generators," Tech. Rep., 2014, p. 36. Accessed: Mar. 1, 2021. [Online]. Available: http://www.wecc.biz/library/WECC Documents/Documents for Generators/WECC Second Generation Wind Turbine Models 012314.pdf
P. Pourbik, "Specification of the second generation generic models for wind turbine generators," Western Electr. Coordinating Council, Salt Lake City, UT, USA, Jan. 2014, pp. 1–36. Accessed: Mar. 1, 2021. [Online]. Available: http://www.wecc.biz/library/WECC Documents/Documents for Generators/WECC Second Generation Wind Turbine Models 012314.pdf
[80] J. Hu, S. Wang, W. Tang, and X. Xiong, "Full-capacity wind turbine with inertial support by adjusting phase-locked loop response," *IET Renew. Power Gener.*, vol. 11, no. 1, pp. 44–53, Jan. 2017.
[81] D. Ramasubramanian, W. Wang, P. Pourbeik, E. Farantatos, A. Gaikwad, S. Soni, and V. Chadliev, "Positive sequence voltage source converter mathematical model for use in low short circuit systems," *IET Gener., Transmiss. Distrib.*, vol. 14, no. 1, pp. 87–97, Jan. 2020.
[82] J. Ma, Z. Song, Y. Zhang, Y. Shen, and J. S. Thorp, "Model order reduction analysis of DFIG integration on the power system small-signal stability considering the virtual inertia control," *IET Gener., Transmiss. Distrib.*, vol. 11, no. 16, pp. 4087–4095, Nov. 2017.
[83] J. Z. Zhou, H. Ding, S. Fan, Y. Zhang, and A. M. Gole, "Impact of short-circuit ratio and phase-locked-loop parameters on the small-signal behavior of a VSC-HVDC converter," *IEEE Trans. Power Del.*, vol. 29, no. 5, pp. 2287–2296, Oct. 2014.
[84] L. Fan and Z. Miao, "An explanation of oscillations due to wind power plants weak grid interconnection," *IEEE Trans. Sustain. Energy*, vol. 9, no. 1, pp. 488–490, Jan. 2018.
[85] L. Papangelis, M.-S. Debry, T. Prevost, P. Panciatici, and T. Van Cutsem, "Stability of a voltage source converter subject to decrease of short-circuit capacity: A case study," in *Proc. Power Syst. Comput. Conf. (PSCC)*, Jun. 2018, pp. 1–7.
[86] E. Alves, G. Bergna-Diaz, D. Brandao, and E. Tedeschi, "Sufficient conditions for robust frequency stability of AC power systems," *IEEE Trans. Power Syst.*, vol. 36, no. 3, pp. 2684–2692, May 2021.
[87] R. A. Jabr, "Economic operation of droop-controlled AC microgrids," *IEEE Trans. Power Syst.*, early access, Nov. 23, 2021, doi: 10.1109/TPWRS.2021.3130128.
[88] M. Ahmed and Y.-C. Kim, "Hierarchical communication network architectures for offshore wind power farms," *Energies*, vol. 7, no. 5, pp. 3420–3437, May 2014.